Identification of Born-Oppenheimer potential energy surfaces of diatomic molecules from optimized chirped pulses

Bjarne Amstrup [a,b], Gábor J.Tóth [b,c], Herschel Rabitz [c] and András Lőrincz [b]

[a] *Chemistry Department B, Technical University of Denmark, DTU–206, DK–2800 Lyngby, Denmark*

[b] *Department of Photophysics, Institute of Isotopes of the Hungarian Academy of Sciences, P.O. Box 77, H-1525 Budapest, Hungary*

[c] *Department of Chemistry, Princeton University, Princeton, New Jersey 08544, USA*

The optimal control of molecules has been widely studied in recent years. In this paper we explore the feasibility of applying adaptive feedback optimal control to determine Born-Oppenheimer (BO) surfaces. If the molecular wave packet is well localized, laser pulses optimized to transfer population between two surfaces contain information on the potential energy difference in the region scanned by the wave packet in the duration of the pulse. By iterating the experiment with the different values of the nuclear separation large regions of the unknown BO surface can be measured if one of the surfaces is known. The method is simulated with a model experiment on CsI. The results show that the BO surface can be determined with reasonable accuracy. Some limitations and possible extensions of the method are discussed.

1 Introduction

The possibility of using external laser fields to control specific chemical reactions or to excite molecules into prescribed states has received considerable attention in recent years; for a recent review see, e.g., [1]. After the pioneering work of Tannor, Rice and Kosloff [2,3] and Brumer and Shapiro [4,5] much theoretical work has been done to establish the feasibility of molecular control. Peirce, Dahleh and Rabitz developed a way of applying the methods of optimal control theory (OCT) to quantum chemical problems which has become the standard formulation of the problem in recent years [6]. A similar

formulation was developed by Kosloff *et al.* [7].

An important step toward laboratory implementation was taken by Judson and Rabitz [8]. They developed a method which, in its extreme form, did not use any *a priori* information of the system being controlled, rather they used an adaptive feedback method, based on a genetic algorithm (GA), to let the laser learn to achieve control of the system. Another adaptive formulation suggests simulated annealing (SA) for laboratory implementations [9]. Earlier OCT methods (i) assumed exact knowledge of the system to be controlled, (ii) used that knowledge to design an appropriate laser pulse and (iii) assumed it would be possible to realize that pulse with great precision in the laboratory. The adaptive feedback method requires (i) a laser which can be controlled to produce suitable pulses, (ii) a measurement system capable of observing the success of control and (iii) an adaptive algorithm which can find the optimal control settings based on the measured success of previous pulses.

Adaptive schemes are highly suitable for laboratory implementation for several reasons. Most importantly, they do not presuppose a detailed knowledge of the quantum system under control, e.g., the exact Hamiltonian of the system. Adaptive algorithms can also overcome the problem posed by the aging of laboratory equipment as they monitor a change of performance and can constantly correct the control. Similarly, the systematic errors and noise inevitable present in the laboratory can to a considerable extent be tolerated by adaptive algorithms [10].

While *a priori* knowledge on the system to be controlled is not needed, the learning process may make some *a posteriori* information available, i.e., the control learned may contain information on the system controlled. In the present paper we derive a way of extracting information on the Born-Oppenheimer (BO) surfaces of molecules. We assume that (i) there is a BO surface other than the electronic ground state that is known with sufficient precision, (ii) the BO surface to be studied is well separated from other surfaces.

The scheme is then the following. The molecule is prepared to be in a well localized state on the known surface, outside the region to be studied, so that either its momentum or the slope of the BO surface is pointing toward the region to be studied. It is allowed to evolve freely for some time (time delay), then it is dumped to the unknown surface with a weak field pulse optimized to give the highest transfer rate.

Analyzing the frequency spectrum of the optimal dumping pulse, we can extract information on the potential energy difference between the two levels in the region covered by the wave packet during the shot, provided that the wave packet is sufficiently localized: the instantaneous frequency of the dumping pulse should at each time instant equal the difference between the two

surfaces at the point where the wave packet was, i.e., at the expected value of the nuclear separation [11]. Repeating the experiment with different values of the delay allows for larger regions to be mapped.

The comparative merits of inversion techniques based on time resolved and frequency resolved (CW) data (such as [12]) has been the topic of much debate. At present, the CW measurements usually provide higher accuracy, allowing more precise inversion, but the accuracy of time resolved measurements is increasing. Moreover, time resolved measurements do not require labeling absorption lines that is a notorious source of error in CW spectroscopy. The CW algorithm [12] could be adapted to the time domain data of the type considered in this paper [13], but the algorithm described in this paper is tailored to the present time-dependent situation. Finally, time resolved spectroscopy is especially well suited to studying flat regions of the Born-Oppenheimer surfaces, e.g., repulsive electronic surfaces.

The main advantage of this algorithm compared to other pump-and-probe techniques as suggested in [14] and theoretically elaborated and detailed from the point of view of inversion in [13], is that it allows for the variation of the frequency during individual measurements. Depending on the slope of the potential surface and the initial velocity of the wave packet, the present approach increases the region of the surface that can be studied by a single measurement considerably. This can well compensate for the increase in the number of measurements caused by the optimization process.

In the following section we describe the above method in detail, with some of the technicalities left for the Appendix. The method is demonstrated for a model experiment on the CsI molecule (Sec. 3). The paper is closed by suggesting the direction for further studies in Sec. 4.

2 The algorithm

As outlined in the Introduction the basic scheme is the following. The molecule is prepared in a well localized state on the known surface, outside the region to be studied, so that either its momentum or the slope of the BO surface is pointing toward the region to be studied. After some time delay a second pulse is deployed to dump the wave packet to the surface to be studied.

If the dumping pulse is weak then the more its instantaneous frequency matches the energy difference at the position of the wave packet the higher the transfer rate will be. Therefore we can optimize the dumping pulse to give the highest transfer rate, with either the amplitude fixed or with the amplitude dependence taken into account. The optimal pulse directly provides the energy

difference between the two electronic surfaces as a function of time. Taking into account the equation of motion of the wave packet allows the potential difference as a function of the nuclear separation to be computed, which directly gives the unknown surface. These calculations are further discussed in the Appendix.

The above scheme requires that the wave packet be highly localized during the transfer; otherwise the notion "the position of the wave packet" is not well defined. In many cases this can be achieved by simply starting from the ground state of the molecule, which is in most cases well localized, and transferring the population to the other known surface. If the time delay is short, the molecule may remain sufficiently localized. However, if this method fails, other methods can be used to prepare the molecule into a well defined localized state [15,16].

To facilitate the successful optimization, the possible control pulses should be coded in a way that is (i) experimentally realizable and (ii) compact, i.e., a small number of parameters suffices. Recent studies [9,17,18] suggest that the chirp expansion is such a coding scheme. The chirp expression of an electric field is

$$\mathcal{E}(t) = \Re\left\{ A\sqrt{\frac{\tau}{2}} \int \exp\left[\mathrm{i}\omega t - \frac{\tau}{4}(\omega-\omega_0)^2 - \mathrm{i}z \sum_{k=0}^{\infty} \frac{\beta^{(k)}}{k!}(\omega-\omega_0)^k \right] \mathrm{d}\omega \right\}. \tag{1}$$

The above expression reflects a possible experimental realization of the pulse: it can be achieved by propagating a Gaussian pulse of the form

$$\mathcal{E}_0^d(t) = \Re\left\{ A\exp(-t^2/\tau + \mathrm{i}\omega_0 t) \right\}, \tag{2}$$

through a medium with a frequency dependent propagation factor β (e.g., an optical fiber) of length z. In both equations $\Re$ denotes the real part of the complex number. Present day experimental possibilities limit the expansion to the first few terms. However, as shown in the Appendix, the instantaneous frequency of a short third order chirped pulse is a quadratic function of time and that is sufficient if the potential energy function can be approximated by a quadratic function in the region covered by the wave packet during the dumping pulse. The zeroth and first derivatives of the propagation factor (i.e., $\beta^{(0)}$ and $\beta^{(1)}$) give a phase factor and a group delay. The second term $\beta^{(2)}$ causes a linear shift in the central frequency and the third term $\beta^{(3)}$ gives rise to some beating in the pulse and is responsible for the quadratic shape of the instantaneous frequency.

The success and effectiveness of the method largely depends on the optimization algorithm used. Optimization algorithms are often divided into two

classes: local and global algorithms, depending whether they search for a local optimum or the global one. As local methods are usually much faster then the global ones, in many cases it is preferable to find a good quality local optimum quickly, compared to finding the global optimum in much longer time. However, for the inversion we need to know the global optimum and local methods can not be acceptable.

An often used global search technique is the genetic algorithm (GA). The GA is a biologically inspired heuristic [19]. It maintains a number of possible solutions, called "individuals" in this context, which are collectively called the "population". A run of the algorithm proceeds as follows. At the beginning the individuals are chosen randomly. Then these individuals are tested for their impact. After the testing is complete each member of the population is allowed to have "offspring", which are generated from it by so called genetic operators. The process then continues with testing of the new "generation".

In most cases the GA works on bit strings as they facilitate a straightforward expression of the genetic operators. The bit strings have to be mapped onto the problem domain one is using. In function optimization, as well as in optimal control, where the goal is to find the best values of some parameters, it is usually done by cutting the string into as many parts as the number of variables, and then interpreting each part as a fixed point number.

When forming a new generation a mating pool is filled with individuals from the previous generation where they are manipulated by the genetic operators; the individuals thus formed constitute the members of the new generation. Operator selection is used first to fill the pool. It serves to give individuals, and through them regions of the search space, of better quality more weight in the search. It is implemented by choosing individuals into the pool in proportion to their fitness. Then cross over is applied to combine partial solutions contained in different individuals to produce individuals potentially fitter than either of the "parents". It can be implemented by cutting the pair of individuals at the same position and then interchanging the half strings (this is called single-point cross over). Generally cross over is not applied to all individuals: pairs of individuals undergo cross over with probability p_x. Mutation is used to maintain a level of diversity in the population by flipping each bit with probability p_{mut}.

The fitness that the selection operator uses can either be the measured success of the control or some function thereof. In practice it is usual to use a linear function of the measured value. The parameters of the scaling function are chosen so that the expected number of offspring of the best individual is at most a given number (α), usually two or three. This so called linear scaling is applied in the present model.

As an optimal pulse will provide information about the BO surface only in a relatively small region, studying larger regions means that the optimization must be conducted many times with different values of the time delay. While it is possible to run the optimization separately each time, it may be much more effective to exploit the fact that the potential energy surface is continuous and thus optimal pulses corresponding to close regions are similar. If we run the optimization processes in parallel, the similarity can be exploited by the use of a new genetic operator: migration [20]. The migration operator is used when all of the GA subpopulations have filled their mating pools. It is applied to each neighboring pair of subpopulations, exchanging each individual in one pool with its corresponding pair in the other one with probability p_{mig}. GA with subsequent migration is called the genetic algorithm with migration (GAM). It may be worth noting that the GAM algorithm could be used even if the potential energy surface had discontinuities; migration makes use of the continuity, but it does not rely on it.

Setting the time delay with great precision can, in some cases, be difficult. The error caused by uncertainty at setting the time delay can be decreased if the time delay can be measured during or after the experiment. One can then discretize the region covered by the time delay by any of the numerous self-organizing methods, such as the Kohonen algorithm [21], and assign a discretization point to each of the subpopulations. Self-organizing will automatically compensate for any systematic error in setting, as the discretization point corresponding to each of the subpopulations is the true average value of the time delay used in optimizing the individuals in that subpopulation. The effect of noise can be decreased by rejecting tests where the time delay delivered is far from the mean value of the corresponding subpopulation.

3 Demonstration

The inversion algorithm proposed in the previous section was tested on a simulated experiment. The experiment was carried out on a model of the CsI molecule, taking into account two BO surfaces: the electronic ground state and an excited state. The excited state was assumed to be known and the ground state was measured. However, no special feature of the ground state is used, any other surface, other than the one from which the molecule is being dumped, can be determined.

The time-dependent Schrödinger equation is

$$\mathrm{i}\hbar\partial_t\Psi(x,t) = \widehat{\mathrm{H}}\Psi(x,t)\,. \tag{3}$$

Within the semi-classical radiation and adiabatic dynamical approximations,

the Hamiltonian may be written as

$$\hat{\mathrm{H}} = \hat{\mathrm{H}}(x,t) = \begin{pmatrix} \hat{\mathrm{H}}_u(x) & -\mu(x)\mathcal{E}(t) \\ -\mu(x)\mathcal{E}(t) & \hat{\mathrm{H}}_g(x) \end{pmatrix} \tag{4}$$

with

$$|\Psi\rangle = \begin{pmatrix} |\psi_u\rangle \\ |\psi_g\rangle \end{pmatrix} . \tag{5}$$

The subscript g and u refer to the "ground" and "upper" state BO surfaces, respectively. $\hat{\mathrm{H}}_i = \hat{\mathrm{T}} + \mathrm{V}_i(x)$ where $\hat{\mathrm{T}} = \hat{p}^2/2m$ is the kinetic energy operator and V_i is the corresponding potential energy. μ is the projection of the transition dipole moment operator onto the direction of the electric field polarization and $\mathcal{E}(t)$ represents the amplitude of the classical electric field. The numerical method used was the split operator method [22,23]. The ground state wave function was calculated by the method of Kosloff and Tal-Ezer [24] through integration of the time dependent Schrödinger equation in imaginary time. The parameters characterizing the model and the numerical method are summarized in Table 1. The physical quantities are given in atomic units, i.e. in terms of $E_h = 219\,474.64\,\mathrm{cm}^{-1}$, $\hbar/E_h = 0.024\,188\,8\,\mathrm{fs}$, $a_0 = 5.291\,77 \times 10^{-11}\,\mathrm{m}$ and $1\,\mathrm{E}_h/(ea_0) = 5.142\,21 \times 10^{11}\,\mathrm{V/m}$.

The molecule is excited to the upper state by an optimized pulse producing 95% inversion [11]. The objective was set to

$$I_p = \int_0^\infty |\psi_u(x,t_1)|^2\,\mathrm{d}x - \lambda_s \int_{t_0}^{t_1} \mathcal{E}_s^2(t)\,\mathrm{d}t, \tag{6}$$

where t_1 is a suitably chosen time after the end of the pumping pulse. $\mathcal{E}_s(t)$ is a sine squared electric field of a given pulse duration, τ_s:

$$\mathcal{E}_s(t) = \mathcal{E}_0^p \sin^2(\pi t/\tau_s)\left[a_1\cos(\omega_s t) + a_2\sin(\omega_s t)\right]. \tag{7}$$

The parameters optimized were $\mathcal{E}_0^p$, a_1, a_2 and ω_s. The pulse duration was chosen to be 20 fs and λ_s was 0.05. The result of the optimization was $\omega_s = 30507\,\mathrm{cm}^{-1}$ and $\mathcal{E}_0^p = 0.0252\,E_h/(ea_0) = 1.296 \times 10^{10}\,\mathrm{V/m}$ corresponding to a maximum intensity $I = \varepsilon_0 c(\mathcal{E}_0^p)^2 = 45\,\mathrm{TW/cm}^2$.

The optimization of the dumping pulses was done by the GAM method. In general, the amplitude of the dumping field can be fixed as it has no effect

Table 1
The parameters of the potentials and the grid used in the simulation of CsI dynamics [18].

Ground potential	Excited potential
$V_g = a\,\mathrm{e}^{-\beta r} - \frac{E_h a_0}{r - r_1}$	$V_u = \mathrm{e}^{-d(r-r_e)}\,E_h - \frac{C_6}{(r-r_2)^6} + V_\infty$
$a = 131.569\,E_h$	$d = 2.571\,02\,a_0^{-1}$
$\beta = 1.370\,42\,a_0^{-1}$	$r_e = 4.20\,a_0$
$r_1 = 0.893\,631\,a_0$	$C_6 = 10.0\,E_h a_0^6$
	$r_2 = 1.889\,72\,a_0$
	$V_\infty = -0.029\,399\,21\,E_h$
Other parameters	
Dipole moment:	$\mu = 0.3\,ea_0$
Masses:	$m_{\mathrm{Cs}} = 132.909\,\mathrm{amu} \quad m_{\mathrm{I}} = 126.904\,\mathrm{amu}$
Grid:	$N = 256 - 1024 \quad \Delta r = 0.016\,5\,a_0$

on the frequency structure of the field, thus the parameters to be optimized are the central frequency (ω_0) and the second and third order chirp ($z\beta^{(2)}$ and $z\beta^{(3)}$). It is thus possible to use a simpler objective function:

$$I_d = \int_0^\infty |\psi_g(x, t_2)|^2\,\mathrm{d}x, \tag{8}$$

where t_2 is a suitably chosen time after the end of the dumping pulse. In the simulations presented here we did optimize the amplitude, keeping the generality of the algorithm being important for other problems, such as [11], so I_d was divided by the energy carried by the pulse and, for convenience, subsequently rescaled:

$$I_d = \frac{E_h \hbar}{e^2 a_0^2} \frac{\int_0^\infty |\psi_g(x, t_2)|^2\,\mathrm{d}x}{\int_{t_1}^{t_2} \mathcal{E}^2(t)\,\mathrm{d}t}\,. \tag{9}$$

The values of the parameters characterizing the algorithm are summarized in Table 2.

A note should be made on the parameters of the GAM. The number of individuals in each subpopulation was fairly low (5). This was possible because the problem domain was relatively easy for the GA. To compensate for this

Table 2
The parameters of the GAM. For efficiency, migration and mutation probabilities were decreased after 50 generations; the two numbers refer to their initial and the final values.

Number of best individual's offspring (α)	2.5
Probability of cross over (p_x)	0.7
Probability of mutation (p_{mut})	0.01/0.005
Probability of migration (p_{mig})	0.01/0.001
Number of subpopulations	20
Number of individuals per subpopulation	5
FWHM of pulse in equation (2) ($2\sqrt{\ln 2}\,\tau$) [fs]	20
Range in which the time delay ($z\beta^{(1)}$) varied [fs]	350–440
Range in which the amplitude (A) varied [$E_h/(ea_0)$]	1.25×10^{-5}–
	-3.75×10^{-5}
Range in which the second order chirp ($z\beta^{(2)}$) varied [$(\hbar/E_h)^2$]	$\pm 10^6$
Range in which the third order chirp ($z\beta^{(3)}$) varied [$(\hbar/E_h)^3$]	$\pm 3 \times 10^8$
Range in which the central frequency (ω_0) varied [$E_h/\hbar$]	0.0644–0.0756

low number of individuals initially a high level of mutation and migration was used, but decreased after 50 generations. In general larger subpopulations are used, which allows a smaller level of mutation and migration to be applied. In practice all these parameters can be tuned to give the best performance.

The optimal solutions found by the GAM after a total of 15,000 trials are listed in Table 3. The solution for the two largest values of the time delay are apparently bad: the central frequency found by the algorithm is the edge of the search interval. In simulations we could simply increase the range for the central frequency, but this may well not be possible in experiments, where the limitations are likely due to the equipment used. One has to be aware of such limitations when evaluating the results.

A typical optimal pulse is shown in Fig. 1 along with its Husimi transform. The Husimi transform of the electric field is defined as

$$G(\omega, t) \propto \int_{-\infty}^{\infty} \mathrm{e}^{-\mathrm{i}\omega(t'-t)}\, \mathrm{e}^{-\gamma(t'-t)^2}\, \mathcal{E}(t')\, \mathrm{d}t', \tag{10}$$

Table 3
The optimal solutions for the different values of the time delay.

$z\beta^{(1)}$ [fs]	$\frac{1}{2}z\beta^{(2)}$ $[10^3\,(\hbar/E_h)^2]$	$\frac{1}{6}z\beta^{(3)}$ $[10^6\,(\hbar/E_h)^3]$	ω_0 $[E_h/\hbar]$
354	−127	3.73	0.074678
359	−135	2.16	0.074282
359	−135	2.16	0.074282
367	−143	0.59	0.072921
368	−143	0.59	0.072921
375	−124	2.55	0.071647
380	−124	2.16	0.070944
386	−151	3.73	0.069978
389	−151	1.76	0.069802
393	−151	1.37	0.069187
397	−159	0.59	0.068660
402	−151	0.59	0.067914
407	−171	1.37	0.067299
411	−163	−0.20	0.066816
414	−155	−0.20	0.066333
421	−155	−0.20	0.065454
424	−155	0.59	0.065059
430	−163	−2.16	0.064444
431	−163	−2.16	0.064400
436	−155	−6.47	0.064400

where γ characterizes the fineness of the transformation; here it is chosen as 2×10^{-6} au. Both plots reveal the significant presence of second order chirp. Both these plots and Table 3 show that the third order chirp is not very high, making the approximations of the Appendix valid.

Given the optimal solution and using the formulae of the Appendix we can calculate the Taylor coefficients of the "unknown" ground BO surface within the region determined by the minimum and maximum values of the $z\beta^{(1)}$ time

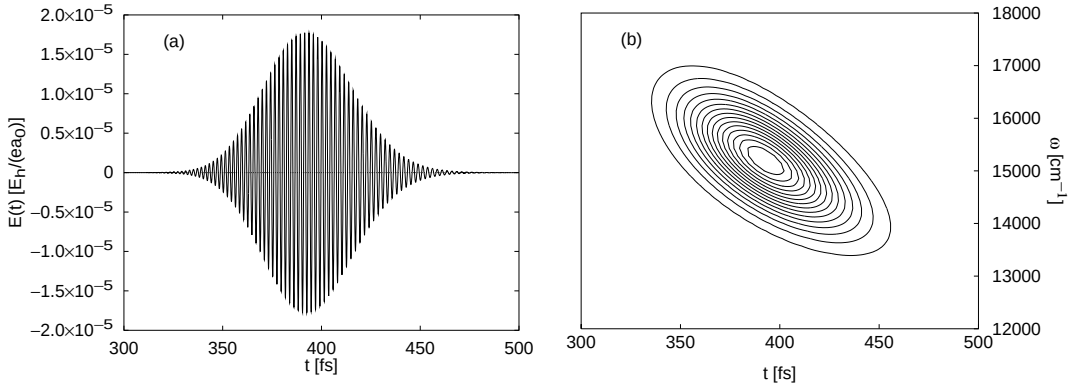

Fig. 1. A typical optimal pulse (a) and its Husimi transform (b).

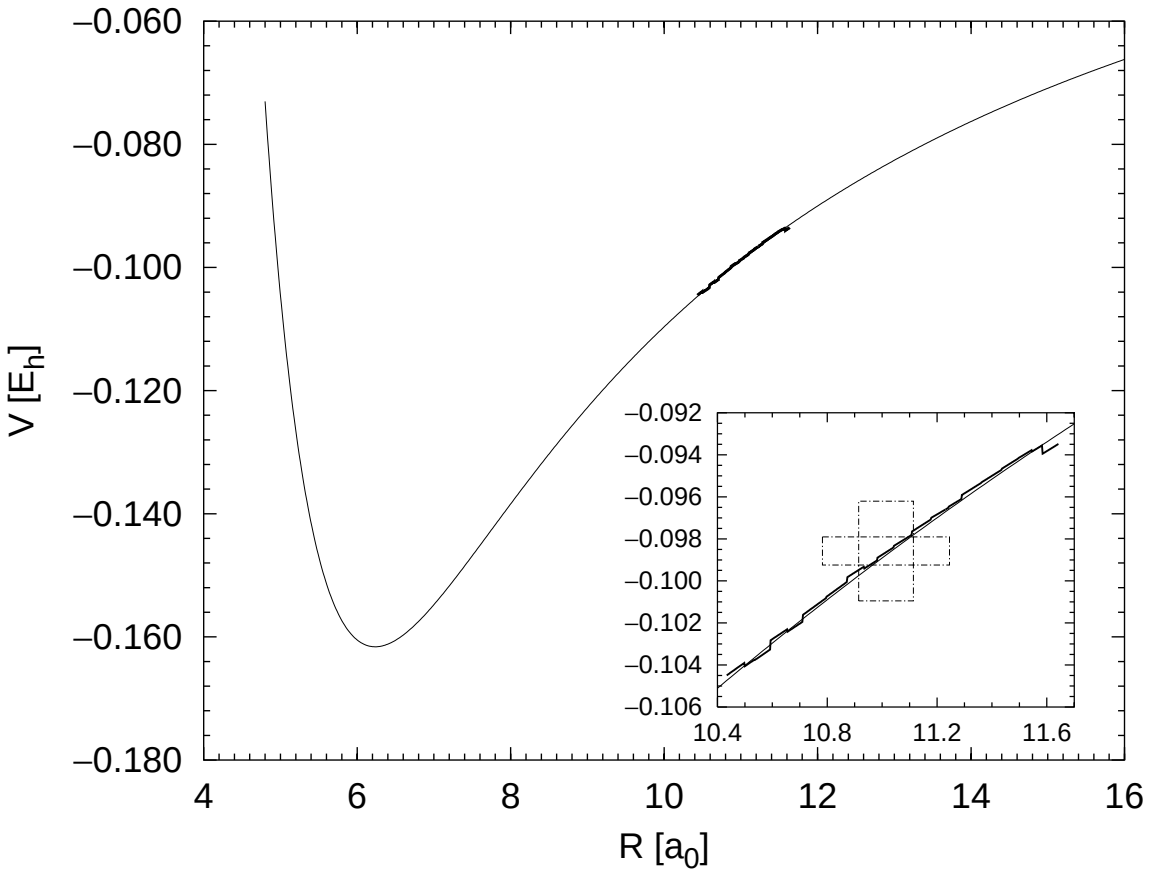

Fig. 2. The reconstructed BO surface (thick line) along with the true one (thin line). The insert shows the uncertainties originating from the pulse (taller rectangle) and the uncertainties originating from the wave-function (shorter rectangle).

delay. The reconstructed BO surface is shown in Fig. 2. The discontinuities of the computed curve arise at border points between different subpopulations; they may be eliminated by numerical smoothing.

The insert of Fig. 2 is an enlarged portion of the lower state potential and the chirped pulse fit of it. The insert has two rectangles. The taller one represents the energy-time uncertainty of the original 20 fs pulse: its vertical size is equal to the the energy uncertainty of the pulse, its horizontal size is equal to the time uncertainty of the pulse multiplied by the velocity of the upper state wave-function when it is at the center position of the rectangle. The other rectangle represents the uncertainties of the wave-function itself: it has a momentum uncertainty and thus a kinetic energy uncertainty - this is the vertical size of the rectangle - and also a position uncertainty - this is the horizontal size of the rectangle. Due to the fitting procedure that has inherent averaging capabilities and to relative structure free nature of the wave-function a good fit could be reached. This underlines the need for localization procedures [15] if the method is to be applied in the general case.

While Fig. 2 shows that the inversion is reasonable, it also reveals the slight tendency to underestimate the gradient of the potential energy difference. This is caused by the relatively large spread of the upper state wave function. As the objective is quadratic in ψ_g (see Eq. 8 or 9) there is a bias to localize the lower state wave-function. Because of the difference between the gradients of the upper and lower state potentials the wave function on the lower state decelerates compared to the upper state. Consequently, the optimal pulse will begin transferring population from the head of the wave packet on the upper state and sweep backward, causing the difference of the gradients of the two potential surfaces be underestimated. This kind of error can be reduced by increasing the localization of the upper state wave function, as suggested in Sec. 2.

4 Conclusion

In recent years much research has been done to control quantum mechanical systems to achieve specific objectives. The tools developed can also be of use to get information on the system controlled. In this paper we described a way of determining a Born-Oppenheimer surface of a molecules. The paper should be regarded as the first step along this direction, with a number of questions left for future research.

Probably the most important limitation of the approach in its present form is the need to know one BO surface with precision. Although such knowledge is in many cases available, an extension of the model may work even in its absence: running a pair of experiments with the role of the two levels exchanged can give enough information to calculate both surfaces. The feasibility of this extension is currently being studied.

Another question open to research is an effective way of controlling the speed and the dispersion of the wave packet. As it can be seen from (30) and (31) very small speeds make the method imprecise. Very large speeds, on the other hand, make the region spanned by the wave packet when the pulse is on very large, which again limits the precision. Large spatial dispersion has a similar effect. To give the best results we therefore need to control the spread and the velocity simultaneously. The bond-locking technique of [16] may be a viable approach, but its applicability needs to be investigated.

Acknowledgement

Part of this work was supported by The Danish Natural Research Science Council, the OTKA Grant of the Hungarian Academy of Science (OTKA 1890/1991), the US-Hungarian Joint Fund Grant (#168a) and the Office of Naval Research.

Appendix

In the Appendix we derive the equations necessary to determine the parameters describing the BO surfaces from the chirp parameters. As the frequency pattern of a third order chirped pulse is characterized by three parameters we can extract three parameters of the BO surface that we chose as the first three Taylor coefficients.

In the following we will assume that the wave packet can be treated classically and talk about its position and velocity, but it is understood that this is only an approximation: in general both the position and the velocity is known with only finite precision, and that both of them cannot be determined simultaneously.

First we calculate the instantaneous frequency of the third order chirped pulse. For convenience we set the zeroth order chirp to zero, as it gives a mere phase factor. Also, we choose the pulse to be centered around $t = 0$, consequently the first order chirp also vanishes from the equation. Thus from (1) we get

$$\mathcal{E}(t) = A\sqrt{\frac{\tau}{2}}\,\mathrm{e}^{\mathrm{i}\omega_0 t} \int_{-\infty}^{\infty} \exp\left\{\mathrm{i}\omega t - \left(\frac{\tau}{4} + \mathrm{i}\frac{z\beta^{(2)}}{2}\right)\omega^2 - \mathrm{i}\frac{z\beta^{(3)}}{6}\omega^3\right\} \mathrm{d}\omega. \quad (11)$$

This integral can be calculated exactly [25], but the resultant expression is too complex to allow simple computations. However, for moderate speed and

gradient values the third order chirp should be small, thus the integral can be approximated by replacing $\exp(-\mathrm{i}z\beta^{(3)}\omega^3/6)$ with its first order Taylor expansion, $1-\mathrm{i}z\beta^{(3)}\omega^3/6$. Using (3.462.2) and (3.323.2) in [26] we get

$$\begin{aligned}\mathcal{E}(t) &\approx A\sqrt{\frac{\tau}{2}}\,\mathrm{e}^{\mathrm{i}\omega_0 t}\int_{-\infty}^{\infty}\exp\left\{\mathrm{i}\omega t-\left(\frac{\tau}{4}+\mathrm{i}\frac{z\beta^{(2)}}{2}\right)\omega^2\right\}\left(1-\mathrm{i}\frac{z\beta^{(3)}}{6}\omega^3\right)\,\mathrm{d}\omega\\ &= A\sqrt{\frac{2\pi\tau}{\tau+2\mathrm{i}z\beta^{(2)}}}\,\mathrm{e}^{\mathrm{i}\omega_0 t}\,\mathrm{e}^{-t^2/(\tau+2\mathrm{i}z\beta^{(2)})}\left\{1+\frac{2z\beta^{(3)}}{3}\frac{t(3\tau+6\mathrm{i}z\beta^{(2)}-2t^2)}{(\tau+2\mathrm{i}z\beta^{(2)})^3}\right\}.\end{aligned} \tag{12}$$

The instantaneous frequency of the field is the time derivative of the phase of the field:

$$\omega_c(t)=\frac{\mathrm{d}\arg[\mathcal{E}(t)]}{\mathrm{d}t}=\omega_0+\frac{4z\beta^{(2)}}{\tau^2+4(z\beta^{(2)})^2}t+\Delta\omega_c, \tag{13}$$

where $\Delta\omega_c$ is given in terms of new parameters a and b as

$$\begin{aligned}\Delta\omega_c &= \frac{\mathrm{d}}{\mathrm{d}t}\arg(1+a(t^3+bt)),\\ a &= -\frac{4z\beta^{(3)}}{3(\tau+2\mathrm{i}z\beta^{(2)})^3},\\ b &= -\frac{3}{2}\tau-3\mathrm{i}z\beta^{(2)}.\end{aligned} \tag{14}$$

By use of

$$\frac{\mathrm{d}}{\mathrm{d}t}\arg z=\frac{\mathrm{d}}{\mathrm{d}t}\Im(\ln z)=\Im\left(\frac{1}{z}\frac{\mathrm{d}z}{\mathrm{d}t}\right) \tag{15}$$

we get

$$\Delta\omega_c(t)=\frac{-2|a|^2b_it^3+3a_it^2+a_rb_i+a_ib_r}{|a|^2t^6+2|a|^2b_rt^4+2a_rt^3+|a|^2|b|^2t^2+2(a_rb_r-a_ib_i)t+1}\,, \tag{16}$$

where a_r, a_i, b_r, and b_i are the real and imaginary parts of parameters a and b, respectively:

$$a_r=\frac{-4z\beta^{(3)}}{3(\tau^2+4(z\beta^{(2)})^2)^3}(\tau^3-12(z\beta^{(2)})^2\tau)\,, \tag{17}$$

$$a_i = \frac{-4z\beta^{(3)}}{3(\tau^2 + 4(z\beta^{(2)})^2)^3}(-6z\beta^{(2)}\tau^2 + 8(z\beta^{(2)})^3)\,, \tag{18}$$

$$b_r = -\frac{3}{2}\tau\,, \tag{19}$$

$$b_i = -3z\beta^{(2)}\,. \tag{20}$$

Let $\omega(t)$ denote the energy difference between the two BO surfaces at the position of the wave packet:

$$\omega(t) = \Delta V[x(t)]\,, \tag{21}$$

where $\Delta V = V_2 - V_1$, and the pulse transfers the wave packet from V_2 to V_1; in the example of Sec. 3 V_1 is the ground state (V_g) and V_2 is the upper state (V_u). If the pulse is sufficiently short we can approximate both ω_c and ω with their second order Taylor expansion. As the frequency of the optimal dumping pulse matches the energy difference between the BO surfaces at the position of the wave packet, i.e., $\omega(t) = \omega_c(t)$, the Taylor coefficients of ω and ω_c should be equal. From (13) and (16) we get

$$\omega_c(0) = \omega_0 + a_r b_i + a_i b_r\,, \tag{22}$$

$$\left.\frac{\mathrm{d}\omega_c}{\mathrm{d}t}\right|_{t=0} = \frac{4z\beta^{(2)}}{\tau^2 + 4(z\beta^{(2)})^2} - 2(a_r b_i + a_i b_r)(a_r b_r - a_i b_i)\,, \tag{23}$$

$$\left.\frac{\mathrm{d}^2\omega_c}{\mathrm{d}t^2}\right|_{t=0} = 6a_i - 2|a|^2|b|^2(a_r b_i + a_i b_r) + 8(a_r b_i + a_i b_r)(a_r b_r - a_i b_i)^2\,. \tag{24}$$

Differentiating (21) with the help of the chain rule yields ($v_0 = \dot{x}(0)$)

$$\omega(0) = \Delta V(x_0)\,, \tag{25}$$

$$\left.\frac{\mathrm{d}\omega}{\mathrm{d}t}\right|_{t=0} = v_0 \left.\frac{\mathrm{d}\Delta V}{\mathrm{d}x}\right|_{x=x_0}\,, \tag{26}$$

$$\left.\frac{\mathrm{d}^2\omega}{\mathrm{d}t^2}\right|_{t=0} = v_0^2 \left.\frac{\mathrm{d}^2\Delta V}{\mathrm{d}x^2}\right|_{x=x_0} - \frac{1}{\mu}\left.\frac{\mathrm{d}V_2}{\mathrm{d}x}\right|_{x=x_0} \left.\frac{\mathrm{d}\Delta V}{\mathrm{d}x}\right|_{x=x_0}\,, \tag{27}$$

where μ denotes the reduced mass of the molecule. In the last equation we made use of Newton's equation of motion:

$$\ddot{x}(t) = -\frac{1}{\mu}\frac{\mathrm{d}V_2}{\mathrm{d}x}\,. \tag{28}$$

Rearranging these equation and taking into account that $\omega(t) = \omega_c(t)$ we finally get:

$$V_1(x_0) = V_2(x_0) - \omega_c(0)\,, \tag{29}$$

$$\left.\frac{\mathrm{d}V_1}{\mathrm{d}x}\right|_{x=x_0} = \left.\frac{\mathrm{d}V_2}{\mathrm{d}x}\right|_{x=x_0} - \frac{1}{v_0}\left.\frac{\mathrm{d}\omega_c}{\mathrm{d}t}\right|_{t=0}\,, \tag{30}$$

$$\left.\frac{\mathrm{d}^2V_1}{\mathrm{d}x^2}\right|_{x=x_0} = \left.\frac{\mathrm{d}^2V_2}{\mathrm{d}x^2}\right|_{x=x_0} - \frac{1}{v_0^2}\left.\frac{\mathrm{d}^2\omega_c}{\mathrm{d}t^2}\right|_{t=0} - \frac{1}{\mu v_0^3}\left.\frac{\mathrm{d}V_2}{\mathrm{d}x}\right|_{x=x_0}\left.\frac{\mathrm{d}\omega_c}{\mathrm{d}t}\right|_{t=0}\,. \tag{31}$$

References

[1] W. S. Warren, H. Rabitz and M. Dahleh, Coherent Control of Quantum Dynamics: The Dream is Alive, *Science* **259** (1993) 1581–1589.

[2] D. J. Tannor and S. A. Rice, Control of selectivity of chemical reaction via control of wavepacket evolution, *J. Chem. Phys.* **83** (1985) 5013–5018.

[3] D. J. Tannor, R. Kosloff and S. A. Rice, Coherent pulse sequence induced control of selectivity of reactions: Exact quantum mechanical calculations, *J. Chem. Phys.* **85** (1986) 5805–5820.

[4] M. Shapiro and P. Brumer, Laser control of product quantum state populations in unimolecular reactions, *J. Chem. Phys.* **84** (1986) 4103–4104.

[5] P. Brumer and M. Shapiro, Control of unimolecular reactions using coherent light, *Chem. Phys. Lett.* **126** (1986) 541–546.

[6] A. P. Peirce, M. A. Dahleh and H. Rabitz, Optimal control of quantum-mechanical systems: Existence, numerical approximation and applications, *Phys. Rev. A* **37** (1988) 4950–4964.

[7] R. Kosloff, S. A. Rice, P. Gaspard, S. Tersigni and D. J. Tannor, Wavepacket dancing: Achieving chemical selectivity by shaping light pulses, *Chem. Phys.* **139** (1989) 201–220.

[8] R. S. Judson and H. Rabitz, Teaching Lasers to Control Molecules, *Phys. Rev. Lett.* **68** (1992) 1500–1503.

[9] B. Amstrup, J. D. Doll, R. A. Sauerbrey, G. Szabó and A. Lőrincz, Optimal control of quantum systems by chirped pulses, *Phys. Rev. A* **48** (1993) 3830–3836.

[10] G. J.Tóth, A. Lőrincz and H. Rabitz, The effect of control field and measurement imprecision on laboratory feedback control of quantum systems, *J. Chem. Phys.* **101** (1994) 3715–3722.

[11] B. Amstrup, G. Szabó, R. A. Sauerbrey and A. Lőrincz, Chirped pulse control of CsI fragmentation: An experimental possibility, *Chem. Phys.* **188** (1994) 87–97.

[12] H. Heo, T.-S. Ho, K. K. Lehmann and H. Rabitz, Regularized inversion of diatomic vibration-rotation spectral data: A functional sensitivity analysis approach, *J. Chem. Phys.* **97** (1992) 852–861.

[13] R. Baer and R. Kosloff, Inversion of Ultrafast Pump-Probe Spectroscopic Data, *J. Phys. Chem.* **99** (1995) 2534–2545.

[14] R. B. Bernstein and A. H. Zewail, Femtosecond real-time probing of reactions. III. Inversion to the potential from femtosecond transition-state spectroscopy experiments, *J. Chem. Phys.* **90** (1989) 829–842.

[15] T. Szakács, J. Somlói and A. Lőrincz, Optimization of Harmonic Oscillator wavefunction squeezing in pulsed electronic transitions, *Chem. Phys.* **172** (1993) 1–6.

[16] T. Szakács, B. Amstrup, P. Gross, R. Kosloff, H. Rabitz and A. Lőrincz, Locking a molecular bond: A case study of CsI, *Phys. Rev. A* **50** (1994) 2540–2547.

[17] J. Janszky, T. Kobayashi and A. Vinogradov, Phonon squeezing in chirped pulse pump and probe experiments, *Opt. Comm.* **76** (1990) 30–33.

[18] S. Ruhman and R. Kosloff, Application of chirped ultrashort pulses for generating large-amplitude ground-state vibrational coherence: a computer simulation, *J. Opt. Soc. Am. B* **7** (1990) 1748–1752.

[19] D. E. Goldberg, *Genetic Algorithms in search, optimization and machine learning* (Addison Wesley, Reading, MA, 1989).

[20] G. J.Tóth and A. Lőrincz, Genetic Algorithm with Migration on Topology Conserving Maps, *Neural Network World* **5** (1995) 171–181.

[21] T. Kohonen, *Self-organization and associative memory* (Springer-Verlag, New York, 1984).

[22] C. Leforestier, R. H. Bisseling, C. Cerjan, M. D. Feit, R. Friesner, A. Guldberg, A. Hammerich, G. Jolicard, W. Karrlein, H.-D. Meyer, N. Lipkin, O. Roncero and R. Kosloff, A comparison of different propagation schemes for the time dependent Shrödinger equation, *J. Comput. Phys.* **94** (1991) 59–80.

[23] M. D. Feit, J. A. Fleck, Jr. and A. Steiger, Solution of the Schrödinger Equation by a Spectral Method, *J. Comput. Phys.* **47** (1982) 412–433.

[24] R. Kosloff and H. Tal-Ezer, A direct relaxation method for calculating eigenfunctions and eigenvalues of the Schrödinger equation on a grid, *Chem. Phys. Lett.* **127** (1986) 223–230.

[25] M. Miyagi and S. Nishida, Pulse spreading in a single-mode fiber due to third-order dispersion, *Appl. Opt.* **18** (1979) 678–682.

[26] I. S. Gradshtein and I. M. Ryzhik, *Table of Integrals, Series, and Products*, fourth ed. (Academic Press, New York, 1980).